Numerical modeling of interply adhesion in composite forming of viscous discontinuous thermoplastic prepregs

P.D. Mulye, J. Hemmer, L. Morançay, C. Binetruy, A. Leygue, Sebastien Comas-Cardona, P. Pichon, D. Guillon

Numerical modeling of interply adhesion in composite forming of viscous discontinuous thermoplastic prepregs

P. D. Mulye[a,b,*], J. Hemmer[b], L. Morançay[a], C. Binetruy[b], A. Leygue[b], S. Comas-Cardona[b], P. Pichon[c], D. Guillon[c]

[a] *Altair Engineering France, 1300, route des crêtes, WTC Bâtiment 4, Entrée M, 06560 Valbonne, France*
[b] *GeM - Research Institute of Civil Engineering and Mechanics, UMR 6183, CNRS - École Centrale de Nantes, 1 rue de la Noë, 44321 Nantes, France*
[c] *Pôle Ingnierie Polymres & Composite, CETIM, Technocampus Composites, Z.I. du Chaffault, 44340, Bouguenais, France*

Abstract

"Quilted Stratum Process" (QSP®) is a new process in the category of thermoplastic composite forming with the objective to locally strengthen the composite parts by strategically stacking discontinuous UD/woven prepregs while maintaining the short cycle time of about one minute. Interply adhesion arising due to polymer tack plays an important role in QSP® due to the presence of resin-rich layer at the ply-ply interface, inability to use blank holders for prepreg patches and high temperature of forming process where the resin is in melt state. Without modeling interply adhesion in the numerical simulation of their forming, plies delaminate unrealistically without any resistance which in turn results in incorrect final positions of the prepreg patches. Thus, a penalty based, semi-empirical contact model for interply adhesion has been developed and implemented in the industrial finite element code of Altair RADIOSS™ . This model allows sliding of plies over long distance while providing a finite adhesive strength before delamination. It requires minimal characterization for which a measurement method is proposed. The usage of this model in a full scale numerical simulation showed that the final ply positions were predicted with a much better accuracy. Also, the predictions of fibre orientations within individual plies are in good agreement with the experimental observations.

Keywords: forming simulation; thermoplastic prepregs; discontinuous patches; interply adhesion modeling

1. Introduction

The usage of composites parts in modern day industry has been increasing significantly mainly due to their high strength to weight ratio which makes them good candidates for structural components. Forming of ThermoPlastic Composites (TPC) is a process which is well suited for mass production due to its short cycle time of about one minute, ease of recycling of thermoplastics and its ability to create components with complex shapes. Added to this is the capability to perform one shot operations on the components without any significant overhead in process time [1].

*Corresponding author
Email address: pmulye@altair.com (P. D. Mulye)

1.1. *Quilted Stratum Process QSP®*

A modified version of the standard thermoplastic composite forming process called "Quilted Stratum Process" (QSP®) [1] has been developed recently. The main idea behind this process is to use discontinuous UD/woven thermoplastic prepreg patches instead of using uniformly shaped prepreg stack as is the case with standard thermoforming process. Thus, even components with complex geometries and curvatures can be formed by using near-rectangular discontinuous patches. A stack of such prepreg patches (Fig. 1a) can be formed into the final component (Fig. 1b) using QSP® . The patch placement is strategically optimized based on the loading to be experienced by the component. Usage of near-rectangular patches and local strengthening of the components reduce material wastage at the same time creating an optimum component performance.

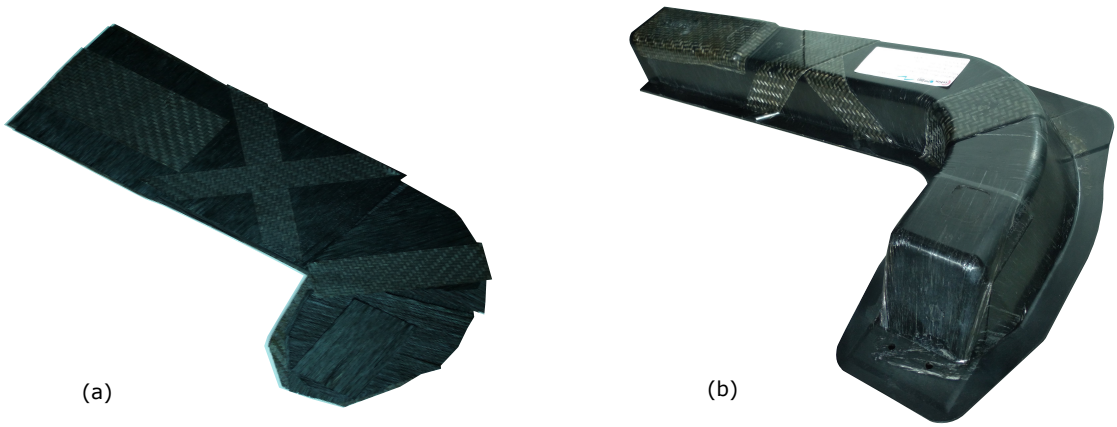

Figure 1: (a) Flat 2D stack of prepregs before QSP® (b) Final formed part

QSP® consists of several sub-steps. At first, the prepreg patches are cut as per requirements and a stack is created with the help of a robotic arm which places the patches at pre-determined locations. The discontinuous patches are spot welded using local heating. After this step, the stack is transferred to an infrared oven where it is heated above the melt temperature of resin. Next, this stack of melt prepreg is transferred to the mold where it undergoes two main stages which are of interest in terms of simulation: forming and consolidation. The main focus of this article is on the forming stage of the process.

Despite the numerous advantages of QSP® described above, there are some challenges associated with the process and subsequently its simulation [2]. These challenges mainly arise due to the unique nature of QSP® . They are as follows:

- Contrary to the standard composite forming process, the use of discontinuous patches makes it impossible to use blank holders.
- QSP® involves an overmoulding process at the end. During the forming and consolidation phases of QSP® , the resin is in melt state due to the high temperature of the process necessary to perform

the overmoulding process later (Fig. 2a). It is important to note that the consolidation step shown in Fig. 2a is not associated with a significant consolidation pressure.

- A resin-rich layer exists at the ply-ply interface [3, 4]. A typical schematic representation of the preform stack for QSP® is shown in Fig. 2b.
- Melt state of resin at the interply interface can result in large sliding (maximum patch sliding reported by [2] is 24.5 mm) and rotation of discontinuous patches.
- QSP® has the capability to create multi-material and multi-thickness components. This however poses a challenges in terms of design of the stack (and patch positions) for QSP® . Challenges associated with the design phase of QSP® known as the "Quilted Stratum Design" (QSD®) are discussed in [5].
- The failure and damage mechanisms for the components manufactured using QSP® need to be studied in order to design the prepreg stack for QSP® [6].

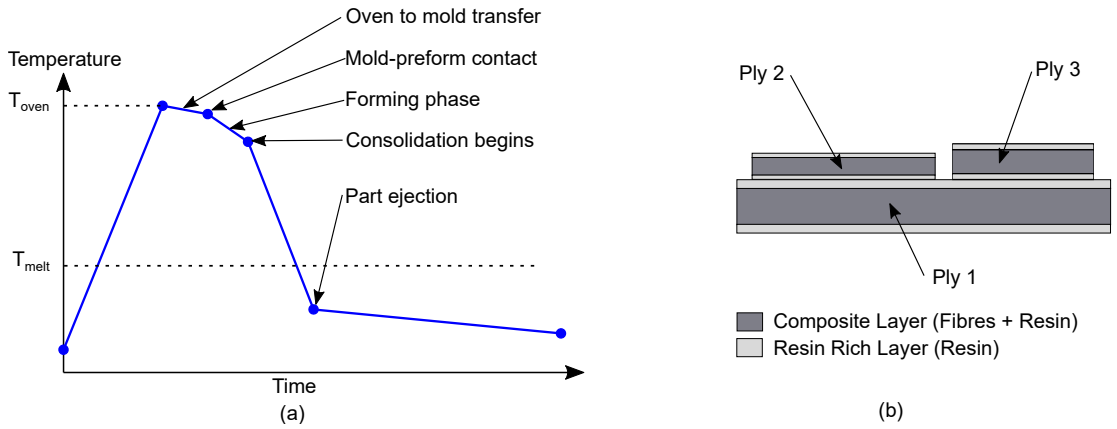

Figure 2: (a) QSP® process temperature evolution (b) Schematic representation of prepreg stack

In order to design the actual component to be manufactured with QSP® , one needs to design the 2D prepreg stack which would then undergo QSP® forming to give the final component. Therefore, a sufficiently good understanding of the mechanisms and physics occurring during the process is needed to obtain the desired final component.

1.2. Interply Adhesion and QSP®

Interply adhesion is one such mechanism which plays an important role in QSP® . It arises from the phenomenon known as *Polymer Tack* which occurs due to the presence of molten resin layer at the ply-ply interface. This phenomenon provides a finite resistance to the interply delamination. The importance of modeling interply adhesion is even more for a process like QSP® due to the absence of blank holder which would otherwise help in keeping the plies together. It was observed that in the numerical

simulation of QSP® , if interply tack is not modeled, the stack of plies unrealistically delaminates without any resistance (Fig. 11a, discussed in detail in Section 5.1). This in turn results in incorrect prediction of the final positions of the discontinuous patches.

Nomenclature wise, the cohesive and adhesive failure can be clearly defined when the system consists of a substrate and an adhesive with a clearly distinguishable boundary between the two. However, in the case of interface between composite plies, it is a little ambiguous due to the presence of resin in a continuous manner. At macro level, it can be called as interply adhesive failure (between plies) even though on the micro level, it is a cohesive failure (more details are given in section 4.1.1).

1.3. Polymer Tack

The term *tackiness* is mainly defined in reference to the adhesives in liquid state. When one tries to transversely separate the solids connected by an adhesive in melt state, tackiness is the resistance offered by the adhesive to the act of separation [7]. The general theory of tackiness for polymers is discussed in [8, 9]. Even though adhesion can originate from various mechanisms such as, mechanical, diffusion, electrostatic and physical/chemical absorption, in regard to the polymer adhesives, the diffusion theory is more relevant [10]. The core idea is that a polymer macromolecule attached to one surface gets diffused into the second surface, creating adhesion between two surfaces.

As one tries to separate the adhesive joint, various mechanisms take place at the interfaces. A detailed experimental analysis was conducted in [11, 12] to study these mechanisms for Pressure Sensitive Adhesives (PSA). Two main parameters quantifying the adhesion were considered, adhesive strength (maximum adhesive stress) and adhesion energy. The debonding process of an adhesive joint consists of several stages, that differs with the debonding rate applied to the sample, as well detailed by Poivet et al. [13] for silicon oils. The rupture can be due to the polymer flow and fingering (low debonding rate) or to cavitation (high debonding rate). In both cases, there is a maximal adhesive measurable force that the sample can handle.

In general, the polymer tack is characterized by measuring the adhesive force response during the debonding phase. A measurement method for tack of polymers was proposed in [14] which involved a layer of polymer deposited on a rigid plate. The flat end of a cylindrical shaped probe made of stainless steel was first brought in contact with this polymer layer. After that, as the probe was pulled in opposite direction (at a controlled debonding rate), the force response was recorded. An ASTM standard for this type of test was proposed in [15] known as the 'Probe Tack Test'. This test technique was used to study the low and high debonding velocity regimes of adhesive failure [13]. It was also used in [16] to measure the force-separation relationship for M21 epoxy resin which was used further to study the local buckling of slit tape for Automated Fibre Placement technique. More recently, this was used by [17] to study the dependence of tack on various parameters for Automated Tape Laying (ATL) process.

A peel-type test was also proposed to measure the tack of prepregs for Automated Tape Laying process in [18, 19]. This test was employed to study the dependence of tack on different parameters in [20]. A floating roller peel test was employed in [21] to measure the polymer tack against the level of cure.

Measurement using peel-type technique is more challenging since it involves correct characterization of other material parameters of prepreg such as bending rigidity which will have a strong influence on the debonding force response.

Several studies have been carried out to measure the adhesion for thermosets (especially on epoxy based) prepregs. The effect of aging and temperature on tack was studied in [22]. A viscoelastic model which requires 4 material parameters was proposed in [23] which was then used to study the tack of epoxy/T-300 carbon fibre reinforced prepregs. For the case of UD-CF/epoxy based system, [24] used Design of Experiments (DOE) to study the effect of impregnation temperature and pressure on tack. The influence of contact time, contact force, temperature, debonding rate and aging on tack was studied in [25]. The adhesion force variation with respect to displacement for the prepreg was compared with the behavior of a pure resin. It was discussed that the behavior difference is seen due to the structural effects in case of prepregs, which mainly arise due to the presence of fibres and non-uniform thickness of resin. Various studies based on DOE were conducted to study the dependency of prepreg tack on various parameters [26, 27].

When it comes to tack of thermoplastic melt prepregs, there is no standard test reported in the literature to the best of the authors knowledge. As a consequence, the interply adhesion created during the QSP® forming phase is, to the authors knowledge, not taken into account in QSP® numerical simulations of thermoplastic prepregs. It is therefore of great interest to propose a novel approach that encompasses numerical and experimental studies to evaluate the influence of the interply adhesion mechanisms on the final spatial positions and orientations of prepreg plies in a full-scale industrial part.

2. Objectives and content of the study

The main objectives of the study are fourfold:

- Propose a simple semi-empirical model that reproduces the interply adhesion between two molten prepreg plies that plays role during the forming phase of the QSP® process.
- Quantify experimentally the adhesive strength of a molten polymer to fuel the interply adhesion model.
- Implement the proposed model coupled with experimental characterization in a full-scale numerical simulation of QSP® to compute the prepreg patch spatial positions and orientations.
- Carry out an extensive comparison between the model's predictions and measurements on a representative industrial part.

After a general presentation of the full-scale simulation strategy, a novel semi-empirical model for prepreg interply adhesion is detailed. Its intentional simplicity requires the characterization of a single parameter which is named *adhesive strength*. Therefore, in a second part, the experimental setup and methodology developed to quantify the adhesive strength of a molten polymer is presented. Thus, the

novel model combined with the experimental data are both integrated in the full-scale numerical simulation of QSP® using Altair RADIOSS™ . The macroscopic numerical results concerning the plies spatial positions and orientations are compared to the experimental results obtained on a full-scale industrial part.

3. Numerical Modeling of Interply Adhesion

Numerical simulation of thermoplastic composite forming process plays a key role in a design of the prepreg stack to be used for forming. A good simulation of a process can avoid the experimental trial and error tests. It therefore has a potential of shortening the process design cycle both in terms of cost and time. Also, with the availability of realistic simulation tools, process parameters can be optimized virtually, using a computer. Thus, a good full scale numerical simulation should be able to capture the physics of the process. At the same time, it should be fast enough to have low impact on overall design time.

Altair RADIOSS™ is an acknowledged industrial FE code used for crash simulation as well as for fluid-structure interaction or stamping process simulation. Due to the in-built rich database of constitutive material models, element formulations, various contact algorithms, scalability and speed; Altair RADIOSS™ code is a very suitable candidate for full scale numerical simulation of composite forming process.

For the numerical simulation of composite forming process, a wide range of approaches exist. A detailed review of these approaches can be found in [28]. Despite the inherent multi-scale nature of the composites, a choice has been made in this work to remain within the scale of macro-level. This choice is made because of the complexity of the components involved in QSP® and computational performance. The main objective of the numerical simulation of QSP® consists of predicting the final position of the discontinuous plies and the fibre orientations in individual plies.

The focus of this work is on the forming stage of QSP® . In simulation, each individual ply is modeled with shell elements at the mid-surface of the ply. The main idea in this work is to replace the resin-rich layer at the interface with an equivalent contact law. This modeling choice has been motivated by the following factors:

- The explicit modeling of resin rich layer results in very expensive computation [4] making it challenging to be used in full scale industrial models.
- Creating such an interface law instead of explicit modeling of resin would benefit in capturing the possible large sliding/rotations of prepreg patches.
- During the forming stage, it can be considered that there is no significant consolidation pressure. Thus, the mechanisms such as bleeding/percolation/squeeze-flow do not occur, keeping the resin-rich layer thickness more or less the same. A numerical model dedicated towards the consolidation phase of the composite forming process is discussed in [29].

There have been several different approaches in the literature aimed at numerical modeling of interply adhesion. One possibility of using cohesive zone elements was discussed in [30]. However, the possible large sliding/rotations make this approach not suitable for QSP® simulation. Interface adhesion limited by a deactivation distance was considered in [31]. In this work, an educated guess has been used to assign the values for the adhesion strength (`0.1` MPa) and the deactivation distance (`2.0` mm) where the ply thickness was `0.14` mm. This was done due to the lack of availability of a standardized test for characterization of adhesion for thermoplastic melt prepregs. [32, 33] modeled interply adhesion with adhesive stiffness and the interply adhesive forces are applied as long as the normal separation between the plies is less than a certain value. The calibration method and the values used for adhesive strength and the deactivation distance are not specified in this work.

Based on the literature review, an interface mechanism providing adhesive strength while permitting large sliding/rotations of plies does not exist. Also, a clear and precise method to characterize such adhesive interface models is needed. Thus, a penalty based, semi-empirical contact model for interply adhesion has been developed and implemented in the industrial finite element code of Altair RADIOSS™ which is discussed in the next section.

3.1. Contact mechanism for interply adhesion

Before getting into the details of the development of the contact mechanism capable of adhesion, it is essential to state the requirements of such a mechanism for it to be suitable for QSP® .

- The model should require the least number of parameters which need characterization. This would make it more suitable for an industry. At the same time, it should have sufficient parameters to capture the physics of the mechanism as closely as possible.
- The model should allow large sliding/rotation of plies while retaining adhesion which is essential for QSP® .
- The model should provide a finite adhesive strength and an ability to delaminate if the normal stress exceeds this value. It should be able to automatically recreate the adhesive bonds if the separated plies come in contact again in future.
- From a point of view of computational performance, the mechanism should be scalable and should work with both Shared Memory Processors (SMP) and domain decomposition with Message Passing Interface (MPI).

As discussed before, the adhesive strength in general depends on many parameters which include, contact time, contact pressure during contact time, debonding rate, temperature, surface characteristics, thickness and nature of the adhesive. However, it is discussed in [34] that as the contact time and contact pressure increase, the adhesive strength becomes almost independent of these parameters. A similar observation was made for debonding rate. When it increases, the adhesive strength asymptotically approaches a constant value. In another work, it was discussed that the effect of surface roughness

diminishes as the contact forces in bonding become high [35]. Also, comparing the force-separation curves in the literature, a general observation can be made about the nature of this curve. The pre-peak behavior is always linear whereas, post-peak behavior varies in general. Based on these observations, a contact algorithm characterized solely by the adhesive strength (σ_{adh}) and linearly increasing force-separation relationship is proposed here.

The modeling strategy for QSP® in Altair RADIOSS™ is to model each individual ply in a prepreg stack (Fig. 3a) with shell elements created at the mid-surface of the solid and to define a standard penalty based node-to-surface contact between the plies (Fig. 3b). As an example, a zoomed in view of the actual component model in Altair RADIOSS™ consisting of 9 plies is shown in Fig. 3c.

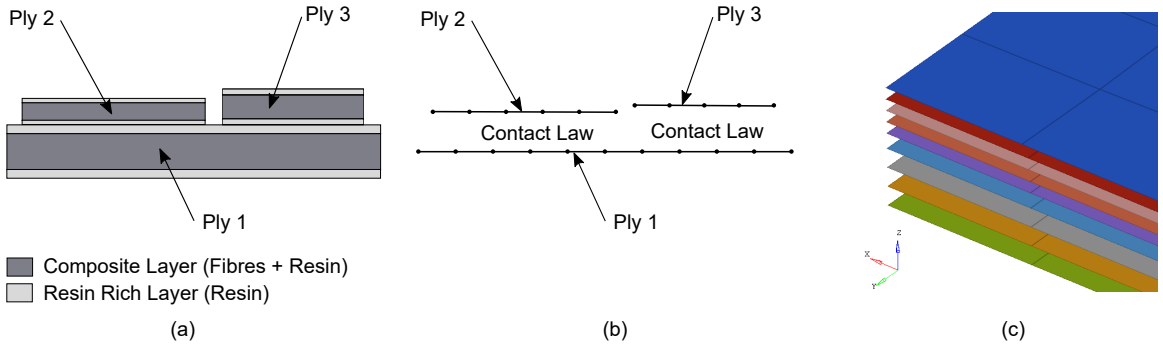

Figure 3: (a) Schematic representation of prepreg stack (b) Modeling strategy for prepreg stack for QSP® in Altair RADIOSS™ (c) Zoomed in view of the actual component with 9 plies modeled in Altair RADIOSS™

In the penalty based contact algorithm defined for the interaction between plies (Fig. 4a), a penetration resistive spring is added whenever the slave node enters the penetration zone. The thickness of penetration zone is given by $L = 0.5 \times (t_{master} + t_{slave})$, where t_{master} and t_{slave} are the thicknesses of master and slave respectively. This standard penalty based contact formulation is modified to have an additional zone of thickness L which extends beyond the penetration zone, called as adhesion zone (Fig. 4b).

The core idea is that, as soon as the slave node touches/enters into the penetration zone, an adhesive spring is created. This spring has no effect in the penetration zone. Thus, the mechanism behaves the same as that of the standard contact algorithm inside penetration zone. However, as the slave node tries to move away from the master and comes in the adhesion zone, adhesive spring (whose base is connected at the interface of adhesion and penetration zone) exerts adhesive forces pulling master and slave pair towards each other. A simple linear force-displacement relationship is used which is given by Eq. 1,

$$F_{adhesion} = \frac{\sigma_{adh}\, A}{L}(L - P) \tag{1}$$

Where, σ_{adh} is the adhesive strength, A is the contact area, P is the normal distance measured with reference to the outer boundary of the adhesion zone. As the node is further pulled and it reaches the outer boundary of adhesion zone, adhesion spring ruptures representing delamination. The adhesive spring is recreated in case the slave node enters the penetration zone again.

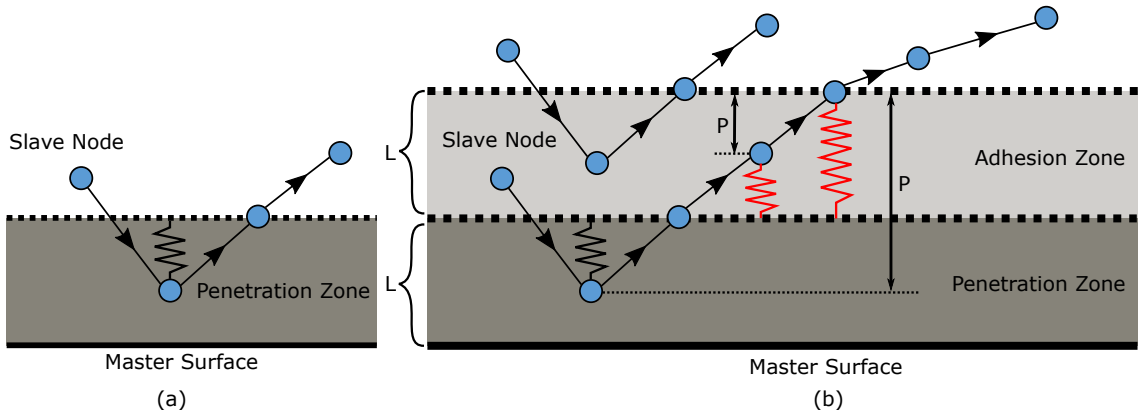

Figure 4: (a) Standard contact mechanism (b) Modified contact mechanism with transverse adhesion

3.2. Mechanism verification with a simple test case

Before using this adhesion mechanism on full scale industrial scenarios, it is tested on a simpler simulation scenario consisting of two flat plates each of thickness `0.5` mm. The plates are modeled with 4 node shell elements created at their respective mid-surfaces (Fig. 5a). The bottom plate (Master) is fixed in all degrees of freedom whereas the top plate (Slave) is subjected to imposed time varying displacement in the normal (z) direction such that the normal interply distance is given by the curve shown in Fig. 5b. The corresponding responses of contact force (N) and contact energy (N.mm) obtained from the simulation are shown in Fig. 6. Note that the values of adhesive strength used in this plot are not real values. In reality, the adhesive stiffness is several orders less compared to the penalty stiffness. Also it is to be noted that this contact mechanism does not require the master and slave nodes to be co-incident, the contact is of type node-to-surface where the penetration on the slave node is calculated based on its projection onto the master surface details of which can be found in [36].

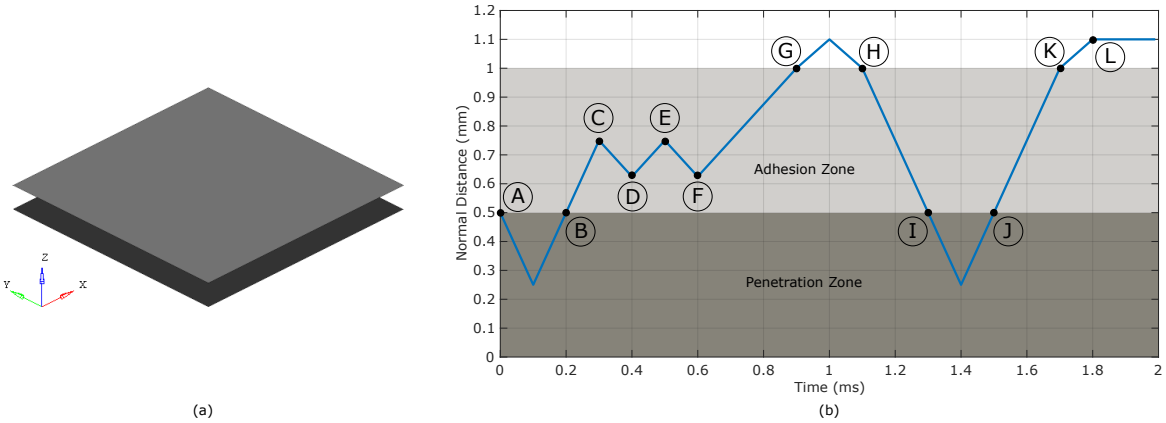

Figure 5: (a) Flat plates geometry and setup (b) Imposed normal interply distance

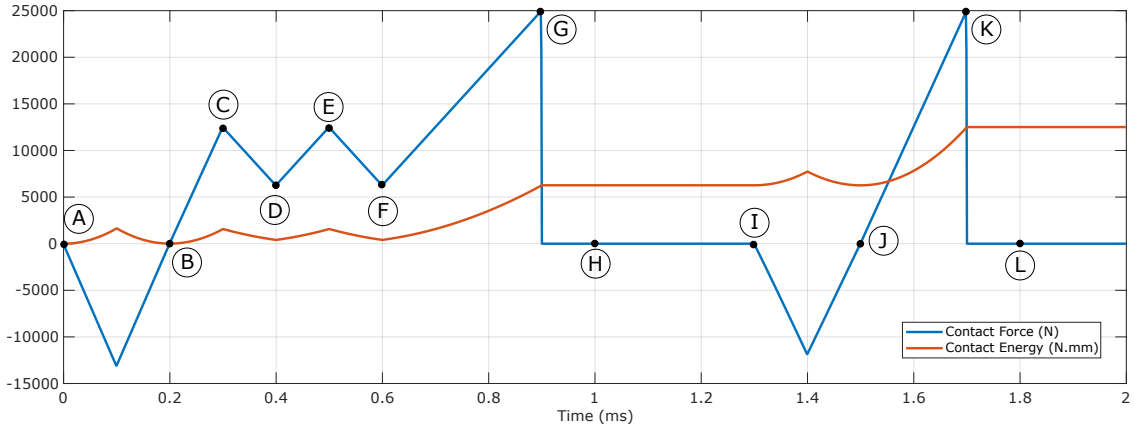

Figure 6: Interply contact force and contact energy obtained from simulation

During the path `A-B`, the plates experience penetration, generating a penetration resistive penalty force which tries to separate master and slave. During this, since the slave node has entered the penetration zone, adhesion spring is created which creates adhesive forces as the slave node enters into adhesion zone (after point `B`). During path `B-C-D-E-F`, this adhesion spring undergoes cycles of stretching and relaxation. The adhesive force which tries to pull master and slave towards one another, possesses an opposite sign as that of penetration resistive forces which can be observed in Fig.6. At point `G`, the adhesion spring is fully stretched (exhibiting maximum adhesion force) and beyond that, it ruptures. It is important to note that after point `H`, even though the top plate enters adhesion zone, the adhesive spring is not recreated until it reaches the penetration zone again (point `I`). Path `J-K` demonstrates the second cycle of increasing adhesion and a rupture at the end. The dissipation resulting from each rupture of the adhesion spring is stored irreversibly in the contact energy which gets accumulated with every cycle of adhesion-rupture.

3.3. Interply contact mechanism in tangential direction

For the full scale implementation, a complete representation of the interface mechanisms is needed. Therefore, in addition to the transverse interply adhesion, a model for tangential interaction between the plies is needed. During the forming phase of QSP® phase, the plies do not experience a significant consolidation pressure. Thus for the interply contact behavior in tangential direction, a viscous slip law discussed in [37] was chosen over the Stribeck curve based approach discussed in [38]. Therefore, irrespective of the zone where a slave node is residing, a tangential force opposing the relative tangential velocity of the slave node with respect to the master is applied. The magnitude of this force is given by Eq. 2,

$$F_T = S\,\frac{\eta\,A}{L}\,(V_{rel}) \tag{2}$$

Where, η being the viscosity of melt thermoplastic resin, A is the contact area and V_{rel} is the tangential

relative speed of the slave node with respect to master. In many full scale industrial models consisting of multiple plies with different ply architectures and fibre orientations, it is difficult to measure the exact thickness (and variation of thickness) of resin rich layer. Therefore, a normalized length L is used in Eq. 2. However, a scaling factor S is provided which can be used to scale-up/scale-down the tangential viscous forces based on the available information about the resin rich layer thickness.

Overall, this mechanism satisfies all the needed requirements described in Section 3.1. However, the mechanism modeled here takes certain computational liberties which were done mainly in order to reduce the characterization needed for modeling the interply adhesion mechanism. First, the post-peak softening behavior of the force-separation behavior is not modeled. Second, the thermal effects are not modeled and finally, the adhesion zone is assumed to be extending up to a normal distance of L. Apart from reducing the needed characterization, this liberty of assuming the adhesion zone thickness was done for one more reason. If the adhesion zone thickness is very small, it will increase contact stiffness significantly (defined by $k_{adh} = \frac{\sigma_{max} A}{L}$) which needs to be taken into account for the stability of the time-step calculation. Therefore, this would result in a very small time-step (which is inversely proportional to the stiffness) for the explicit solver, increasing the computational cost significantly.

4. Experimental determination of the interply adhesion strength

From the characterization point of view, the adhesion model proposed here needs only one main parameter, the adhesive strength (σ_{adh}). After a detailed literature review on polymer rupture, this section describes the developed experimental setup and methodology used to determine the adhesive strength (σ_{adh}) of melt thermoplastic polymer PA-66.

4.1. Literature review

4.1.1. Cohesive or adhesive rupture

A resin-rich layer of `0.1` to `0.5` mm exists at the interface between two plies of prepreg [39] and the rupture occurring when the transverse stress exceeds the transverse maximal strength adhesion σ_{max} may be adhesive (rupture at the interface between the fibrous reinforcement and the resin) or cohesive (rupture in the resin bulk). Bastien et al. [40] investigated the fusion between two graphite/PEEK prepreg plies at molten state using a thin amorphous polyetherimide (PEI) film. Authors highlighted that for a contact time t_c between both components higher than the PEI reptation time τ_{rept} (which sets the self-diffusion rate of the polymer [41]), the transverse rupture occurs in the bulk of the PEI polymer. Experiments conducted on highly entangled polymers lead to similar conclusions [42]. According to molecular dynamics simulations [43], if $t_c < \tau_{rept}$, the polymer entanglement density remains low and leads to chain pull-out (adhesive rupture); in contrast, if $t_c > \tau_{rept}$, the polymer entanglement density is maximal and the cohesive rupture is due to chain scission.

For PA-66, a conventional polymer used to make thermoplastic prepreg, $\tau_{rept} \approx 10^{-5}$ s (obtained following Doi Tube theory [41] and using molecular data from [44]). Before the forming process, the prepreg plies

	Min.	Max.	Resolution
Force (N)	0.002	150	0.000024
Displacement (μm)	1	6000	0.003
Temperature (^{0}C)	T_{Room}	450	0.1

Table 1: Specifications of the force, displacement and temperature cells for the DMA *Metravib*150+

remain stacked at melt temperature during much longer time. Therefore, the transverse rupture between two prepreg plies is expected to be cohesive, *i.e* in the bulk of the molten polymer.

4.1.2. Fluid-like or solid-like rupture

The molten polymer rupture depends on the applied strain rate $\dot{\varepsilon}$ [45], [46]. A low strain rate induces a fluid-like rupture (ductile) whereas a high strain rate induces a solid-like rupture (elastic). When the product $\dot{\varepsilon}\tau_{rept}$ is higher than 1, the polymer macromolecules do not have enough time to reorganize following the imposed strain and the induced rupture is elastic [47], [48]. Schach et al. [42] consider that the transition between fluid-like and solid-like rupture occurs for $\dot{\varepsilon}\tau_{rept}$ varying from 0.8 to 7.

During the forming process, the strain rate $\dot{\varepsilon} \in$ [1-1000] s^{-1} and again, $\tau_{rept} \approx 10^{-5}$ s for PA-66. The cohesive rupture is therefore expected to be fluid-like between two prepreg plies at molten state.

Following the conclusions raised by the present literature review, the strength adhesion between two melt thermoplastic prepreg plies will be investigated through the tensile mechanical behavior of the corresponding molten polymer.

4.2. Experimental methods and setup

Fig. 7 presents the setup developed to measure the transverse tensile mechanical behavior of a molten PA-66 following the methods employed for silicon oils [13]. A Dynamic Mechanical Analysis device (DMA 150+ from *Metravib*) whose specifications are detailed in Table 1 is used as a tensile machine where jaws are two parallel steel platens. A PA-66 sample from Solvay (melt temperature T_m=280$^\circ C$ and melt viscosity 70 Pa.s) is placed on the bottom fixed platen, located in a furnace.

The initial thickness of the molten polymer is set by imposing a compressive constant force (-0.5 N) on calibrated shim plates during 1 minute. Once this bonding step achieved, a constant tensile force rate is imposed and both force and displacement are recorded. The setpoints applied during each step are detailed in Table 2. The sample volume remains constant during the experimental campaign (diameter of 33 mm and thickness of 0.5 mm) and each test is repeated twice at a given force rate.

4.3. Experimental results

Qualitative results obtained on molten PA-66 (Fig. 7b) are in good agreement with the one obtained on silicon oils (Fig. 7c, extracted from [13]). At low debonding velocity, a radially convergent flow is observed (fingering effect) whereas cavitation occurs at high debonding velocity. In QSP® , the debonding rates of

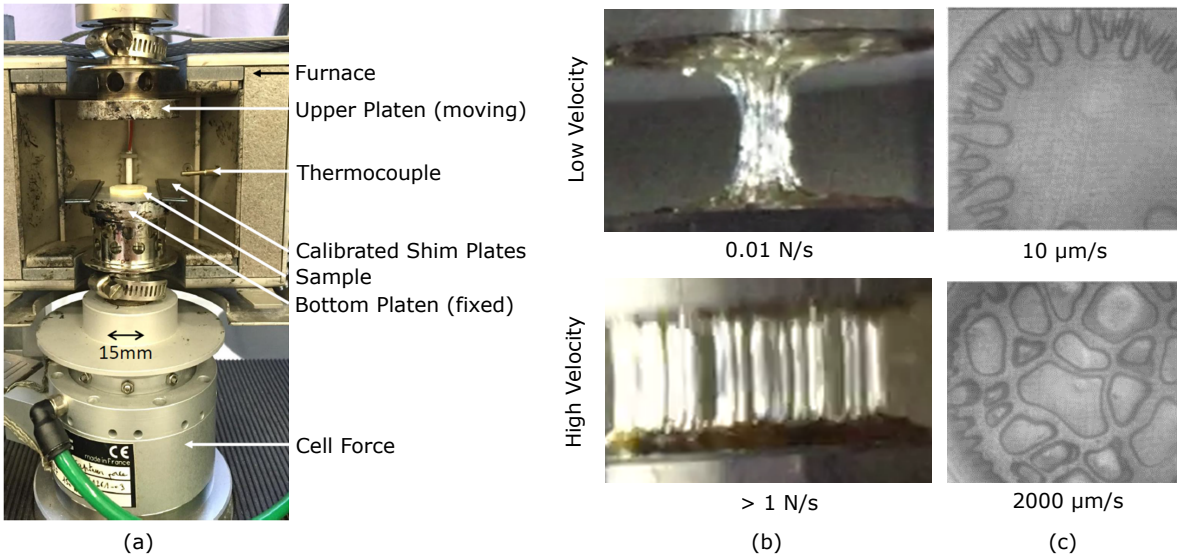

Figure 7: (a) Global view of the setup designed to measure the tensile mechanical behavior of molten PA-66 (b) Experimental evidence of the fingering and cavitation effects occurring respectively at low and high debonding velocities: cross-section views, (c) Top views extracted from [13]

Step	Force	Temperature
Melting	0 N	10^0C/min to T_m
Bonding	-0.5 N	T_m
Tensile	Constant rate from 0.001 to 1 N/s	T_m

Table 2: Experimental protocol steps with the corresponding imposed force and temperature

plies are quite high (discussed in detail in Section 4.4) which indicates that the mechanism consisting of extensional separation is more important compared to the mechanism creating radially convergent flow.

Barroso et al. [45] distinguished the failure (loss of adhesion) happening when the force reaches a maximal peak and the rupture (no polymer threads remain between the two platens) occurring after the failure. This force peak is believed to represent the instability and transition from homogeneous stretching to necking [49] and the use of the Considère criterion to predict it for molten polymer and polymer solutions is still discussed [50], [51]. For the present study, the maximal force is found to be as a good indicator to quantify σ_{max}.

Even if test repeatability is difficult to ensure, the molten PA-66 tensile behavior significantly depends on the imposed force rate (Fig. 8). The sample rupture, not represented here, occurs right after the force peak at high force rate and long after the force peak at low force rate. The force rate significantly impacts the maximal strength adhesion value (σ_{max} in Fig. 9a). Equivalent conclusions are drawn for silicon oils [13]. However, the material viscosity (10^2 to 10^3 Pa.s in [13]) does not influence the force peak value. Therefore, the obtained trend curve (Fig. 9a) can be used to determine the maximal strength adhesion

Debonding rate (1/s)	Adhesive Strength (MPa)
2.00E-04	7.72E-04
6.00E-04	1.40E-03
5.00E-03	2.31E-03
1.50E-02	4.28E-03
4.00E-02	5.75E-03

Table 3: Experimentally obtained values of adhesive strength of PA-66 at high temperature for different debonding rates

for a more viscous PA-66 molten polymer.

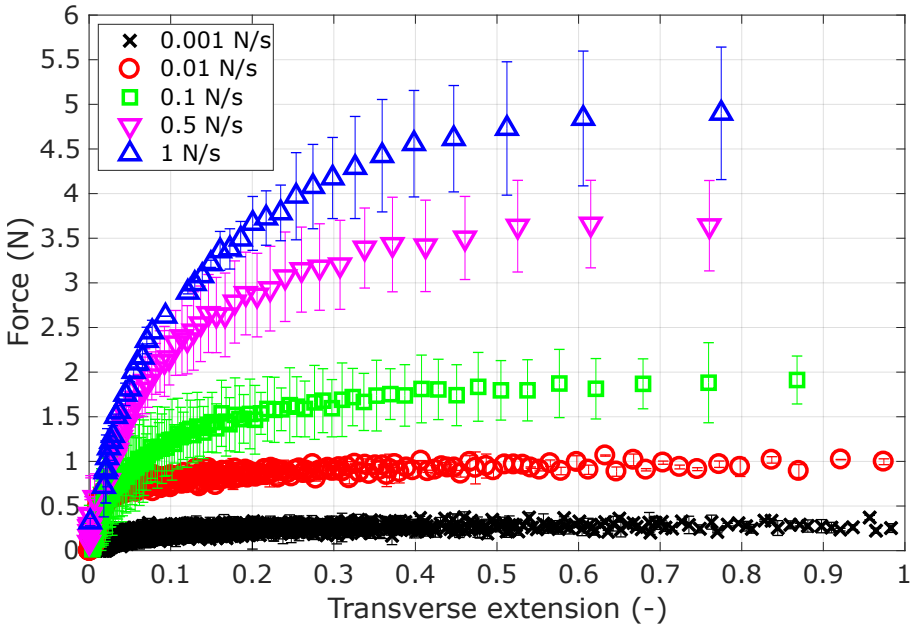

Figure 8: Quantitative results showing the raw force and displacement recorded for several force rates

4.4. Choice of adhesive strength value for simulation

As discussed in [25], the non-uniformity of interfacial resin layer thickness in case of prepregs affects the post-peak behavior of the force-separation curve, however, the linear nature of the pre-peak behavior is still retained. Since, the focus of this article is on pre-peak linear behavior, the adhesion tests conducted on pure resin (Section 3) can be used to model the interply adhesion for thermoplastic prepregs.

As observed from the experiments, the value of the adhesive strength varies with the debonding rate (Table 3). However, it was observed by [34, 12] that at higher debonding rates, the adhesive strength becomes less dependent on the debonding rate. Inspired from this observation, a curve fitting of the form

$y = a(1 - \exp^{-bx}) + c$ was performed (Fig. 9a). The parameters obtained from the curve fitting exercise were $a =$ `0.0052`, $b =$ `67.86` and $c =$ `0.001` which produced an $R^2 =$ `0.9921`. With higher debonding rates, the value of adhesive strength approaches asymptotically to a value of `0.0062` MPa.

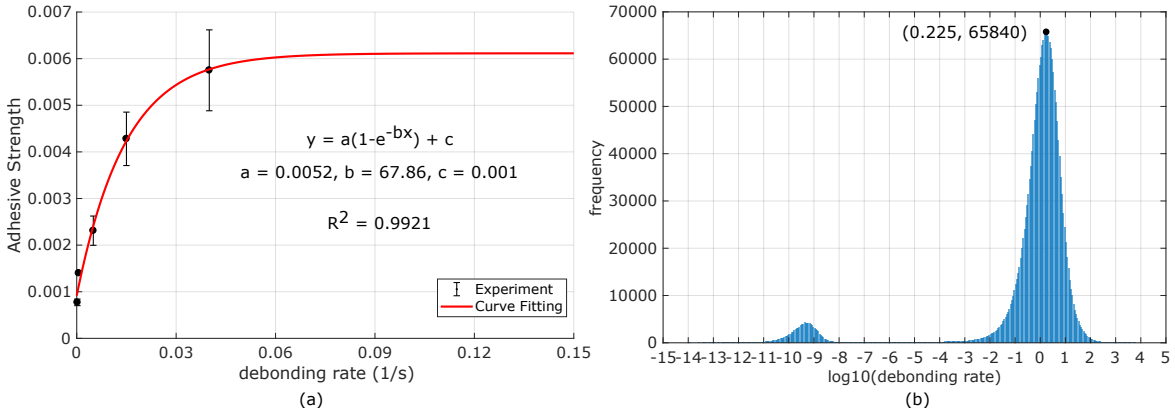

Figure 9: (a) Curve fitting for adhesive strength experimental values (b) Histogram of local debonding rates from simulation

A simulation based study was conducted for an industrial case (model description and setup is described in Section 5) to observe the local instantaneous debonding rate throughout the simulation. The value of local debonding rate was calculated for each node, each contact interface after every `1000` cycles in simulation which resulted in a database of about `2` million data points. A histogram plot (Fig. 9b) for these values shows that the majority of the values occur around the debonding rate of $10^{0.225} = 1.68$ (1/s) for which the adhesive strength can be safely considered to be `0.0062` MPa. This justifies the use of a constant adhesive strength value = `0.0062` MPa in the simulation. The sensitivity analysis of adhesive strength has been performed and is discussed in Section 5.2.

5. Full scale numerical simulation of QSP® using Altair RADIOSS™

This section discusses a numerical simulation of QSP® for an industrial component performed using an explicit dynamics finite elements approach of Altair RADIOSS™ with the added interply adhesion mechanism where a central difference algorithm has been used for time descretization [52, 36].

5.1. Model description and setup

The considered industrial model (Fig. 10a) has a prepreg stack consisting of 9 plies of different shapes, fibre architectures (UD/woven) and fibre orientations (Fig. 10b). This component has been designed by CETIM after doing several initial design iterations. The woven prepreg plies are TEPEX® dynalite `101-RG600(x)` (Supplier: BONDLAMINATES). The UD ply tapes are Celestran® `CFR-TP PA-66 GF60-02` (Supplier: TICONA).

The punch and die are modeled with rigid elements. Each ply is meshed with 4 noded shell elements (created at the mid-surfaces of plies) with hourglass free full integration elements [53]. Since, a prepreg

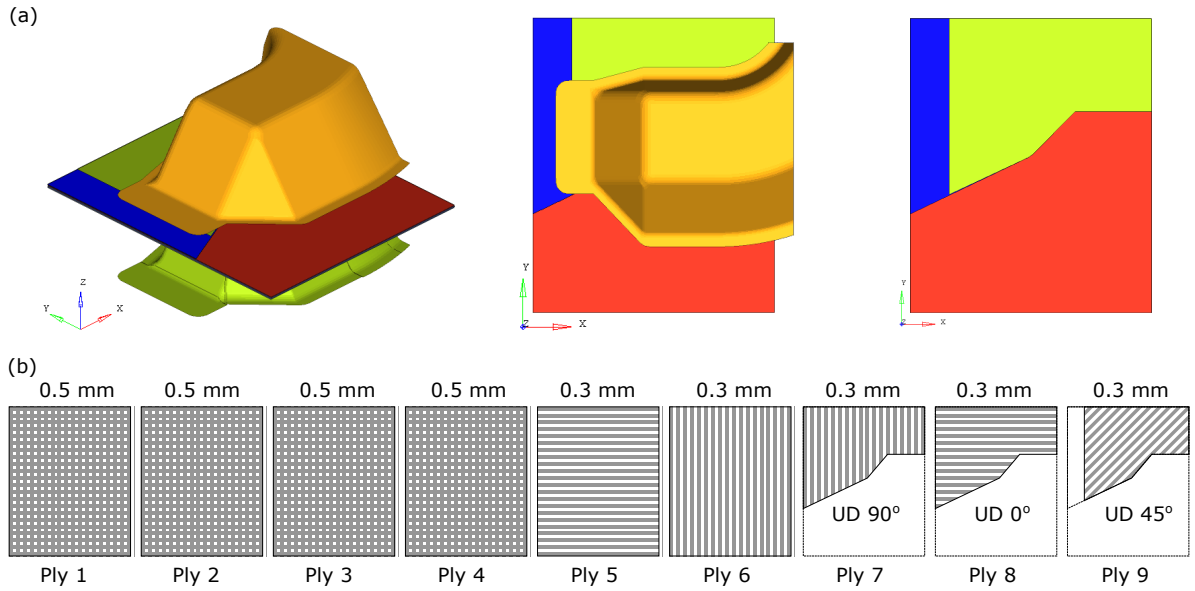

Figure 10: (a) Industrial model geometry and simulation setup (b) Prepreg stack configuration (Ply 1 to 9: from bottom to top in the stack)

ply consists of both fibres and resin, each ply is modeled by overlapping two sets of shell elements with co-incident nodes. One set of shell elements obeys a fabric constitutive model and the other set obeys the resin constitutive model. The mesh size of 4 mm was used which generated a total 29,653 nodes consisting of 48,404 quadrilateral elements.

Constitutive model for fabric behavior has been implemented in material Law-58 of Altair RADIOSS™ which models the fabric as a hyperelastic anisotropic membrane material. On the other hand, the resin behavior is modeled with a constitutive model corresponding to Mooney-Rivlin material which is a particular case of material Law-42 of Altair RADIOSS™ . More details about these constitutive models cane be found in [36]. The material parameters used in the simulation are listed in Table 4 which have been obtained from an experimental campaign. The value of viscosity has been obtained from the specifications provided by the prepreg supplier.

The ply-ply interaction is modeled with a penalty-based contact (Type 25) formulation in Altair RADIOSS™ which has been modified to incorporate interply adhesion developed in this work. Also, specially defined rigid to deformable contacts are defined between the die/punch and plies. The interply adhesion parameters used for the simulation are listed in Table 5.

The simulation was run on a Inter (R) Xeon (R) CPU E5-2680 v3 @ 2.50GHz (x86_64) machine with SPMD=1 and OMP=24 type of parallel environment. The simulation was run with the natural time-step of the model (approximately 3.0E-7 seconds) and in total 113,458 cycles were completed for the total time of 0.034 seconds. The CPU time used in the simulation was found to be 75,350 seconds whereas the actual time taken for the simulation to complete was found to be 3,198 seconds.

Woven (Law-58)		UD (Law-58)		Resin (Law-42)	
ρ	1.8E-9 t/mm^3	ρ	1.8E-9 t/mm^3	ρ	1.13E-9 t/mm^3
E_1	10,000 MPa	E_1	25,000 MPa	ν	0.495
E_2	10,000 MPa	E_2	10 MPa	μ_1	2.0
G_0	0.069 MPa	G_0	0 MPa	μ_2	-1.0
G_T	3.0 MPa	G_T	3.0 MPa	α_1	2.0
α_{lock}	55 degrees	α_{lock}	85 degrees	α_2	-2.0

Table 4: List of parameters for each constitutive model used in simulation where ρ is the density, E_1 and E_2 are the young's modulii of fibres for warp and weft directions, G_0 is the initial shear modulus, G_T is the tangent shear modulus at locking angle α_{lock}. For resin, ν is the poisson's ratio, μ_1, μ_2, α_1 and α_2 are material parameters for the Ogden material law.

Parameter	Symbol	Value
Viscosity of melt resin (280^0 C)	η	275 Pa.s
Adhesive strength	σ_{adh}	0.0062 MPa
Viscous scaling factor	S	1.0

Table 5: List of interply adhesion parameters used in simulation

For a qualitative validation, the ply positions at an intermediate time step were compared for the case without interply adhesion mechanism against the case with interply adhesion mechanism. A resistance free delamination of plies was observed when interply adhesion was not modeled (Fig. 11a). On the other hand, with the added interply adhesion model, the prepreg plies stick together (Fig. 11b). This in

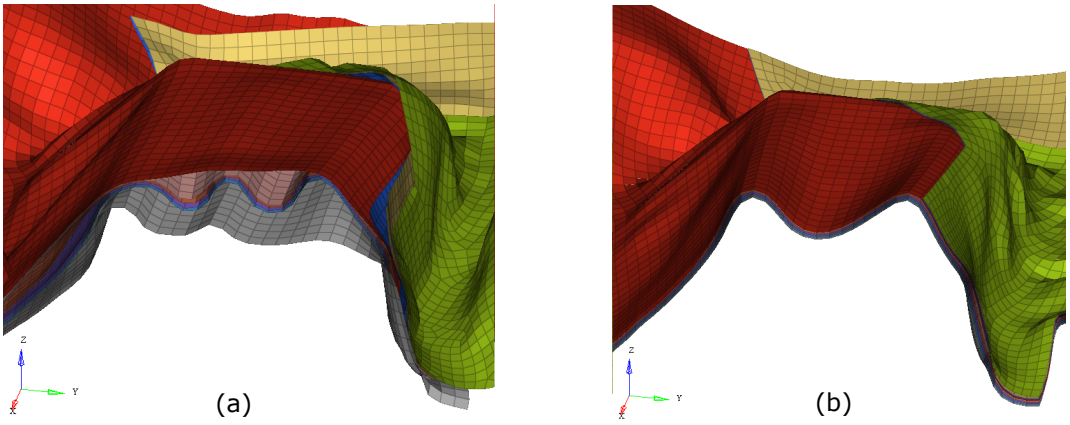

Figure 11: (a) Without interply adhesion: resistance free delamination (b) With adhesion: no delamination

turn affects the final position of discontinuous plies. The positions predicted by the simulation without interply adhesion (Fig. 12a) are significantly different from those predicted by the simulation with interply adhesion (Fig. 12b).

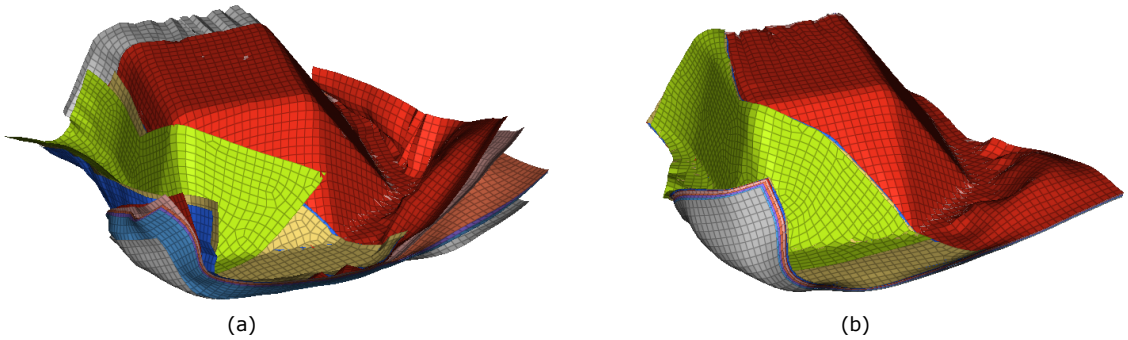

Figure 12: Comparison of the final position of plies (a) Without interply adhesion model (b) With interply adhesion model

The quantitative validation was done by comparing the simulation with the experiments. This was done in two parts (a) Comparison of the final position of a prepreg patch (b) Comparison of fibre orientations for all plies at several locations.

5.2. Comparison of the final position of a prepreg patch

The vertical displacement of a corner (Point P shown in Fig. 13) was measured from the experiments and it was compared with values obtained from the simulation. The experimentally obtained value was 6 mm (Fig. 13a). The simulation without the interply adhesion mechanism predicted this value to be 31.7 mm (Fig. 13b) which is quite different from the real value. On the other hand, adding interply adhesion mechanism improved this value to 6.6 mm (Fig. 13c) which is much closer to the experimentally observed value.

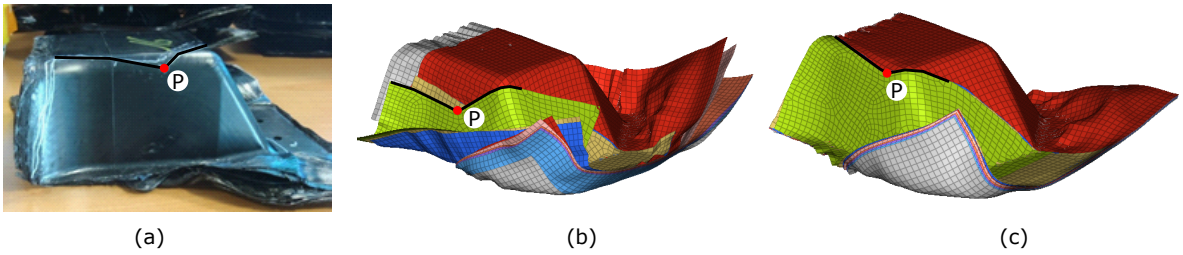

Figure 13: Vertical displacement of a patch corner (a) Experiment: 6 mm (b) Simulation without interply adhesion: 31.7 mm (c) Simulation with interply adhesion: 6.6 mm

Another comparison was made with reference to the angle made by the patch with respect to the horizontal ($\angle ABC$ shown in Fig. 14). Experimental measurements showed that this angle was 60 degrees (Fig. 14a). Note that this change of angle results from the sliding of discontinuous patch and not from in-plane shearing of the prepreg. The simulation without the interply adhesion model predicted it to be

27.9 degrees (Fig. 14b) whereas the simulation with interply adhesion mechanism gave a much closer prediction of 64.4 degrees (Fig. 14c).

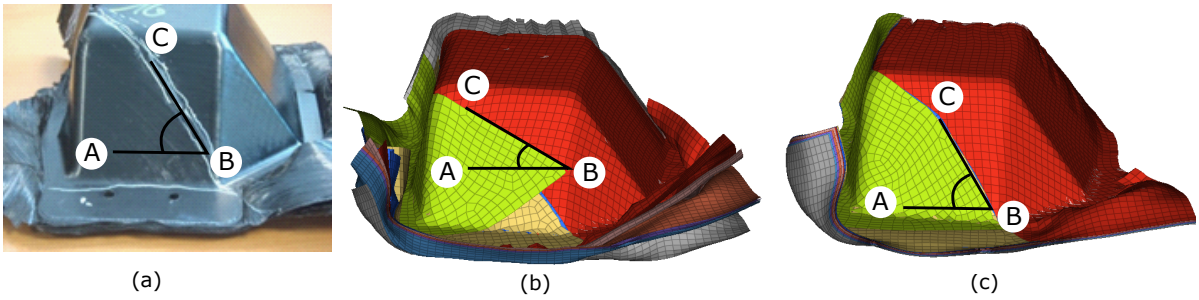

Figure 14: Comparison of the angle made by top ply with horizontal (a) Experiment: 60 degrees (b) Simulation without interply adhesion: 27.9 degrees (c) Simulation with interply adhesion: 64.4 degrees

Therefore, it can be concluded that with added interply adhesion contact mechanism, there is a significant improvement in the prediction of the final ply positions.

A sensitivity analysis was performed on the adhesive strength parameter. The final positions of 6 nodes situated at the corners of Ply 9 (Fig. 15) were recorded by post-processing the simulation results. The simulations were performed by varying σ_{adh} from its reference value of 0.0062 MPa. The variation was performed from σ_{adh} = 0.0012 MPa (reference value -80%) to σ_{adh} = 0.012 MPa (reference value +80%). Table 6 shows the variation of the final position (magnitude) of these nodes in mm with respect to the reference case (σ_{adh} = 0.0062 MPa). In general, σ_{adh} can be thought of as an entity that opposes the separation forces experienced during the forming process. Thus, as long as σ_{adh} exceeds the local separation stress experienced by the plies, the final position of plies remains more of less the same, indicated by the almost similar values of relative distance for positive variation of σ_{adh} in Table 6. On the other hand, if σ_{adh} is less than the local separation stress, there will be local delaminations which can eventually create significant variation in the final position of the plies. This indeed was observed as σ_{adh} value was reduced from its reference value, at the value of 0.0012 MPa, the maximum final position variation was found to be 21.63 mm.

5.3. Comparison of fibre orientations for individual plies

After forming this component using QSP® , the fibre orientations at various locations were experimentally measured for each ply. In order to perform these measurements, the resin was burned off to unstack the laminate. These measurements were verified at several locations using X-ray tomography scanning technique.

The measurement locations are shown in Fig. 16b along with the local coordinate systems used for each face (Fig. 16a). For a quadrilateral face, the measurement locations lie on the diagonals and are 25 mm away from the intersection of diagonals. For a triangular face, the measurement location lies on the angle bisector of the top angle and is located at one third distance from the base of the triangle. In terms

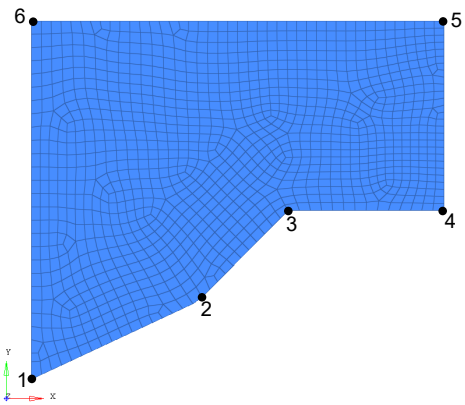

Figure 15: Position measurement locations on Ply 9 for sensitivity study

σ_{adh} (MPa)	0.0012 -80%	0.0037 -40%	0.005 -20%	0.0056 -10%	0.0068 +10%	0.0074 +20%	0.0087 +40%	0.0112 +80%
Node 1	21.63	5.86	4.29	3.57	2.72	1.14	1.14	1.14
Node 2	2.43	0.61	0.18	0.32	0.07	0.12	0.12	0.12
Node 3	2.66	0.66	0.27	0.27	0.07	0.27	0.27	0.27
Node 4	2.37	0.43	0.55	0.24	0.48	1.16	1.16	1.16
Node 5	0.51	0.38	0.67	0.71	0.32	0.11	0.11	0.11
Node 6	4.07	2.03	1.92	0.72	0.44	0.72	0.72	0.72
Average	5.61	1.66	1.32	0.97	0.68	0.59	0.59	0.59
Maximum	21.63	5.86	4.29	3.57	2.72	1.16	1.16	1.16

Table 6: Sensitivity of adhesive strength

of nomenclature for Fig. 16b, a generic location is globally identified with two numbers I.J, where I indicates the face and J indicates the location on Ith face. For a woven fabric prepreg, the orientation of both the fibre families was recorded. This in total resulted in 186 data points. These values are compared with the fibre orientations at the same locations for the simulation with added interply adhesion contact model (σ_{adh} = 0.0062 MPa).

The fibre orientations measured from the experiments at these locations were compared with the values obtained from the simulation. The results summarized with respect to each face are presented in Table 7. Detailed information can be found in Appendix in Table A.8 and Table A.9. It can be seen that for Faces 1, 4, 5 and 6, almost all values from simulation are in quite a good agreement with the experimental observations. For Face 2, even though the overall predictions are in good agreement, there are some locations where some difference can be observed. One hypothesis for this difference is potentially in the horizontally flat nature of this face which would mean that other mechanisms such

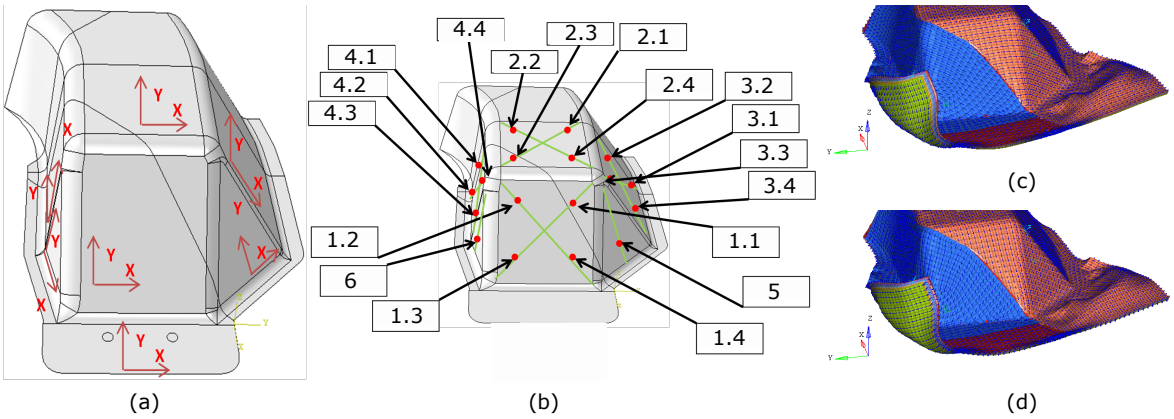

Figure 16: Fibre orientation comparison information (a) Local coordinate systems (b) Measurement locations (c) Simulation with adhesion: Fibre direction 1 (d) Simulation with adhesion: Fibre direction 2

Face	Data Points	Average of absolute difference (degrees)
1	39	3.9
2	40	5.1
3	40	9.8
4	44	5.6
5	10	3.2
6	13	5.1

Table 7: Summary of fibre orientation comparison for each face

as squeeze flow, resin bleed can play a key role on this face as shown in [4]. However, this hypothesis needs further investigation. For Face 3, all values are in good agreement with an exception of just one location (Location 3.4 in Table A.8 and Table A.9) where the simulation differs significantly from the experiments. This in turn has increased the average of absolute difference for this face. Authors believe that this is an experimental measurement anomaly at this location since the fibre orientations for all other locations (and all plies) on this face are quite close to the predictions from the simulations. Overall, the fibre orientations predicted by the simulation were on an average 5.9 degrees away from the experiments.

6. Conclusion

In this work, the importance of modeling interply adhesion for QSP® has been demonstrated. It is worth to recall the peculiarities of this process that make the usual models not suitable: (a) usage of discontinuous prepreg patches (b) inability to use a blank holder (c) long distance sliding of patches during the forming phase. Thus, a novel semi-empirical contact mechanism to model this phenomenon has been developed which creates a finite adhesive strength for ply-ply contact. At the same time, it

allows sliding of plies along with automatic recreation of adhesion if the plies come in contact again. In terms of computational performance, the model has been implemented for shared memory processors (SMP) as well as for domain decomposition with MPI in Altair RADIOSS™ showing its scalability.

In terms of characterization, the interply adhesion numerical model proposed here just requires the values of adhesive strength and viscosity of melt resin. This makes it highly suitable for industrial applications where an extensive characterization campaign is often a challenge in terms of cost and time. A detailed experimental procedure has been developed to quantify the interply adhesive strength of molten thermoplastic polymer.

Finally, it has been shown that, using this novel numerical model of interply adhesion coupled with adapted experimental data, the prediction of final positions of the plies has improved significantly. Also, the fibre orientation predictions are shown to be in good agreement with the experimental observations made on full-scale industrial QSP® parts. Thus to conclude, this numerical model of interply adhesion has improved the numerical simulation of composite forming of viscous discontinuous thermoplastic prepregs.

7. Acknowledgements

The authors would like to express their gratitude towards ANRT (CIFRE #2017/1621) for the financial support. The authors would also like to thank CETIM for providing the experimental information related to the industrial model used in this work.

Appendix A. Fibre orientations data from experiment and simulation

The nomenclature for the tables is as follows: A point (at which fibre orientation is measured) is identified as `PiDj` where `i` denotes the ply number and `j` denotes the family of fibres (1 or 2). The column `Loc` contains the identifier for the measurement location of plies (Refer to Fig. 16)

Loc	P1D1	P1D2	P2D1	P2D2	P3D1	P3D2	P4D1	P4D2	P5D1	P6D1	P7D1	P8D1	P9D1
1.2	-1.0	93.7	-3.0	91.5	0.5	92.5	94.0	3.3	98.0	15.7	15.7	106.7	147.0
1.3	3.7	93.3	-1.5	92.5	1.5	91.5	92.3	1.0	94.7	4.0	4.0	101.3	147.0
1.4	6.3	92.0	2.0	94.0	0.0	96.5	99.3	-1.7	94.7	5.3	5.3	98.3	140.3
2.1	3.0	92.0	7.5	93.5	17.5	95.5	92.3	16.3	88.0	2.7			
2.2	1.7	89.3	15.5	88.5	14.0	86.0	80.3	15.7	81.7	1.3			
2.3	0.3	91.0	-10.0	92.5	-10.0	93.5	92.3	-11.7	85.3	1.7			
2.4	7.3	93.0	12.5	91.5	13.5	93.5	94.0	14.3	89.3	2.3			
3.1	11.7	100.7	13.5	102.5	24.0	104.5	104.7	28.3	96.3	16.3			
3.2	14.7	98.3	18.5	91.5	29.5	87.5	90.0	30.3	90.0	16.7			
3.3	14.7	97.3	18.5	100.5	24.5	102.0	96.3	32.7	92.3	17.0			
3.4	11.0	105.7	21.0	107.5	26.5	106.0	103.3	29.3	105.3	17.3			
4.1	167.7	84.0	161.0	85.0	152.0	84.5	87.0	152.0	83.3	158.3	158.3		
4.2	170.0	83.3	163.0	84.0	160.0	81.0	76.3	158.0	75.7	162.7	162.7		
4.3	166.3	78.3	164.0	57.5	154.0	59.0	63.7	152.7	65.3	155.3	155.3		
4.4	165.7	81.0	163.0	78.0	153.0	75.5	76.3	151.7	77.0	155.7	155.7		
5	128.0	72.5	130.5	66.0	135.5	66.5	69.5	136.5	75.0	135.5			
6	71.5	127.0	64.5	120.0	59.0	128.0	129.0	54.5	133.0	62.5	62.5	135.0	23.0

Table A.8: Fibre orientations (in degrees) measured from experiments

Loc	P1D1	P1D2	P2D1	P2D2	P3D1	P3D2	P4D1	P4D2	P5D1	P6D1	P7D1	P8D1	P9D1
1.2	1.9	100.0	2.6	99.4	3.1	100.0	100.0	3.3	100.1	6.6	9.1	106.2	147.5
1.3	4.1	96.4	4.8	96.5	5.6	97.0	97.6	6.7	98.7	10.4	11.3	99.7	134.4
1.4	3.7	95.1	2.1	95.3	1.4	95.7	95.9	1.4	95.9	-3.8	6.2	97.9	140.3
2.1	8.8	97.3	3.9	95.8	22.0	97.5	96.5	16.9	97.0	-13.8			
2.2	-2.8	88.0	22.3	85.2	-2.0	84.3	85.0	11.7	84.9	1.2			
2.3	4.1	87.8	3.1	87.7	3.2	88.2	88.4	2.2	88.5	-1.2			
2.4	6.5	92.9	6.1	93.2	5.6	93.3	93.7	4.9	94.5	7.3			
3.1	25.5	96.1	25.4	96.0	25.8	95.8	95.8	26.8	96.3	26.7			
3.2	23.5	99.2	26.1	98.0	26.3	97.3	96.7	26.7	96.1	27.9			
3.3	27.2	102.1	26.5	103.2	27.2	103.3	104.3	27.6	104.3	27.1			
3.4	25.7	137.6	25.6	137.4	26.5	138.0	138.1	26.9	136.9	27.1			
4.1	157.5	79.8	157.7	80.2	154.6	78.8	82.4	155.4	79.7	157.6	157.0		
4.2	167.8	78.5	166.2	82.5	163.0	79.6	76.3	161.5	79.7	161.2	161.3		
4.3	157.9	50.5	158.0	50.7	157.2	49.5	49.1	158.0	48.3	158.7	159.1		
4.4	153.7	72.2	153.5	68.2	153.5	68.1	67.8	153.3	69.9	152.5	154.3		
5	136.3	69.8	135.9	70.2	135.9	70.6	70.9	135.8	70.4	135.9			
6	66.1	132.2	64.7	131.7	64.7	131.8	131.9	64.1	132.0	62.3	61.8	133.4	5.2

Table A.9: Fibre orientations (in degrees) measured from simulation

References

[1] D. Guillon, A. Lemasçon, C. Callens, QSP® : An innovative process based on tailored preforms for low cost and fast production of optimized thermoplastic composite parts, in: ECCM 2016 - Proceeding of the 17th European Conference on Composite Materials, 2016.

[2] J. Schell, L. Amory, D. Guillon, Movement of patches during thermoforming: Experiment and simulation, in: AIP Conference Proceedings, Vol. 1769, AIP Publishing, 2016, p. 170032.

[3] F. N. Cogswell, 4 - the microstructure of aromatic polymer composites, in: F. N. Cogswell (Ed.), Thermoplastic Aromatic Polymer Composites, Butterworth-Heinemann, 1992, pp. 78–106.

[4] G. Sorba, C. Binetruy, A. Leygue, S. Comas-Cardona, Squeeze flow in heterogeneous unidirectional discontinuous viscous prepreg laminates: Experimental measurement and 3d modeling, Composites Part A: Applied Science and Manufacturing 103 (2017) 196–207.

[5] Irisarri, François-Xavier and Macquart, Terence and Julien, Cédric and Espinassou, Denis, A novel design method for the fast and cost-effective manufacture of composite parts employing the Quilted Stratum Process, Composites Part B: Engineering 158 (2019) 364–372.

[6] Todeschini, Y and Huchette, C and Julien, C and Espinassou, D, Analysis of damage and failure mechanisms of Quilted Stratum Process composite parts, in: ECCM17 - Proceeding of the 17th European Conference on Composite Materials, Munich, Germany, 2016.

[7] J. Bikerman, The fundamentals of tackiness and adhesion, Journal of Colloid Science 2 (1) (1947) 163–175.

[8] C. Gay, Some fundamentals of adhesion in synthetic adhesives, Biofouling 19 (S1) (2003) 53–57.

[9] C. Gay, Stickinesssome fundamentals of adhesion, Integrative and comparative biology 42 (6) (2002) 1123–1126.

[10] K. Allen, Adhesion and adhesives–some fundamentals, Studies in Conservation 29 (sup1) (1984) 5–12.

[11] H. Lakrout, P. Sergot, C. Creton, Direct observation of cavitation and fibrillation in a probe tack experiment on model acrylic pressure-sensitive-adhesives, The Journal of Adhesion 69 (3-4) (1999) 307–359.

[12] B. Lestriez, H. Lakrout, A. Chiche, A. Roos, C. Creton, Probe tack tests as a characterization tool in pressure-sensitive-adhesives, in: Proceedings of the PSTC Technical Seminar TECH XXIV, Orlando, FL, USA, 2001, pp. 2–4.

[13] S. Poivet, F. Nallet, C. Gay, J. Teisseire, P. Fabre, Force response of a viscous liquid in a probe-tack geometry: Fingering versus cavitation, The European physical journal E 15 (2) (2004) 97–116.

[14] A. Zosel, Adhesion and tack of polymers: Influence of mechanical properties and surface tensions, Colloid and Polymer Science 263 (7) (1985) 541–553.

[15] ASTM, Standard test method for pressure-sensitive tack of adhesives using an inverted probe machine, ASTM D2979–01.

[16] A. Beakou, M. Cano, J.-B. Le Cam, V. Verney, Modelling slit tape buckling during automated prepreg manufacturing: A local approach, Composite structures 93 (10) (2011) 2628–2635.

[17] D. Budelmann, H. Detampel, C. Schmidt, D. Meiners, Interaction of process parameters and material properties with regard to prepreg tack in automated lay-up and draping processes, Composites Part A: Applied Science and Manufacturing 117 (2019) 308–316.

[18] R. Crossley, P. Schubel, N. Warrior, The experimental characterisation of prepreg tack, in: The 17th International Conference on Composite Materials (ICCM-17), 2009.

[19] R. Crossley, P. Schubel, N. Warrior, Experimental determination and control of prepreg tack for automated manufacture, Plastics, Rubber and Composites 40 (6-7) (2011) 363–368.

[20] A. Endruweit, G. Y. Choong, S. Ghose, B. A. Johnson, D. R. Younkin, N. A. Warrior, D. S. De Focatiis, Characterisation of tack for uni-directional prepreg tape employing a continuous application-and-peel test method, Composites Part A: Applied Science and Manufacturing 114 (2018) 295–306.

[21] R. Banks, A. Mouritz, S. John, F. Coman, R. Paton, Development of a new structural prepreg: characterisation of handling, drape and tack properties, Composite Structures 66 (1-4) (2004) 169–174.

[22] K. Ahn, L. Peterson, J. Seferis, D. Nowacki, H. Zachmann, Prepreg aging in relation to tack, Journal of applied polymer science 45 (3) (1992) 399–406.

[23] K. Ahn, J. Seferis, T. Pelton, M. Wilhelm, Analysis and characterization of prepreg tack, Polymer Composites 13 (3) (1992) 197–206.

[24] B. S. Hayes, J. C. Seferis, J. S. Chen, Development and hot-melt impregnation of a model controlled flow prepreg system, Polymer composites 17 (5) (1996) 730–742.

[25] O. Dubois, J.-B. Le Cam, A. Beakou, Experimental analysis of prepreg tack, Experimental Mechanics 50 (5) (2010) 599–606.

[26] J. Putnam, J. Seferis, T. Pelton, M. Wilhelm, Perceptions of prepreg tack for manufacturability in relation to experimental measures, Science and Engineering of Composite Materials 4 (3) (1995) 143–154.

[27] C. Wohl, F. L. Palmieri, A. Forghani, C. Hickmott, H. Bedayat, B. Coxon, A. Poursartip, B. Grimsley, Tack measurements of prepreg tape at variable temperature and humidity, in: Proceedings of Composites and Advanced Materials Expo (CAMX 2017), Orlando, FL; United States, 2017.

[28] P. Bussetta, N. Correia, Numerical forming of continuous fibre reinforced composite material: A review, Composites Part A: Applied Science and Manufacturing 113 (2018) 12–31.

[29] Xiong, Hu and Hamila, Nahiène and Boisse, Philippe, Consolidation Modeling during Thermoforming of Thermoplastic Composite Prepregs, Materials 12 (18) (2019) 2853.

[30] Q. Chen, P. Boisse, C. H. Park, A. Saouab, J. Bréard, Intra/inter-ply shear behaviors of continuous fiber reinforced thermoplastic composites in thermoforming processes, Composite Structures 93 (7) (2011) 1692–1703.

[31] S. Haanappel, Forming of UD fibre reinforced thermoplastics, Ph.D. thesis, University of Twente, Netherlands (2013).

[32] D. Dörr, F. Henning, L. Kärger, Nonlinear hyperviscoelastic modelling of intra-ply deformation behaviour in finite element forming simulation of continuously fibre-reinforced thermoplastics, Composites Part A: Applied Science and Manufacturing 109 (2018) 585–596.

[33] D. Dörr, M. Faisst, T. Joppich, C. Poppe, F. Henning, L. Kärger, Modelling approach for anisotropic inter-ply slippage in finite element forming simulation of thermoplastic ud-tapes, in: AIP Conference Proceedings, Vol. 1960, AIP Publishing, 2018, p. 020005.

[34] A. Gillanders, S. Kerr, T. Martin, Determination of prepreg tack, International Journal of Adhesion and Adhesives 1 (3) (1981) 125–134.

[35] A. Zosel, The effect of bond formation on the tack of polymers, Journal of adhesion Science and technology 11 (11) (1997) 1447–1457.

[36] Altair Engineering, Radioss Theory Manual, 2018.

[37] E. Lamers, Shape distortions in fabric reinforced composite products due to processing induced fibre reorientation, Ph.D. thesis, Netherlands (2004).

[38] U. Sachs, R. Akkerman, K. Fetfatsidis, E. Vidal-Sallé, J. Schumacher, G. Ziegmann, S. Allaoui, G. Hivet, B. Maron, K. Vanclooster, et al., Characterization of the dynamic friction of woven fabrics: experimental methods and benchmark results, Composites Part A: Applied Science and Manufacturing 67 (2014) 289–298.

[39] J.-H. Belnoue, O. Nixon-Pearson, D. Ivanov, S. Hallett, A novel hyper-viscoelastic model for consolidation of toughened prepregs under processing conditions, Mechanics of Materials 97 (2016) 118–134.

[40] L. Bastien, J. Gillespie Jr, A non-isothermal healing model for strength and toughness of fusion bonded joints of amorphous thermoplastics, Polymer Engineering & Science 31 (24) (1991) 1720–1730.

[41] M. Doi, S. F. Edwards, The theory of polymer dynamics, Vol. 73, oxford university press, 1988.

[42] R. Schach, C. Creton, Adhesion at interfaces between highly entangled polymer melts, Journal of Rheology 52 (3) (2008) 749–767.

[43] T. Ge, F. Pierce, D. Perahia, G. S. Grest, M. O. Robbins, Molecular dynamics simulations of polymer welding: Strength from interfacial entanglements, Physical review letters 110 (9) (2013) 098301.

[44] J. E. Mark, Physical properties of polymers handbook, Vol. 1076, Springer, 2007.

[45] V. Barroso, R. Andrade, J. Maia, An experimental study on the criteria for failure of polymer melts in uniaxial extension: The test case of a polyisobutylene melt in different deformation regimes, Journal of Rheology 54 (3) (2010) 605–618.

[46] A. Y. Malkin, C. Petrie, Some conditions for rupture of polymer liquids in extension, Journal of Rheology 41 (1) (1997) 1–25.

[47] Y. Wang, P. Boukany, S.-Q. Wang, X. Wang, Elastic breakup in uniaxial extension of entangled polymer melts, Physical review letters 99 (23) (2007) 237801.

[48] Q. Huang, N. J. Alvarez, A. Shabbir, O. Hassager, Multiple cracks propagate simultaneously in polymer liquids in tension, Physical review letters 117 (8) (2016) 087801.

[49] A. Y. Malkin, A. Arinstein, V. Kulichikhin, Polymer extension flows and instabilities, Progress in Polymer Science 39 (5) (2014) 959–978.

[50] C. J. Petrie, Considère reconsidered: Necking of polymeric liquids, Chemical Engineering Science 64 (22) (2009) 4693–4700.

[51] M. H. Wagner, V. H. Rolón-Garrido, Constant force elongational flow of polymer melts: Experiment and modelling, Journal of Rheology 56 (5) (2012) 1279.

[52] T. Belytschko, W. K. Liu, B. Moran, K. Elkhodary, Nonlinear finite elements for continua and structures., John wiley & sons, 2013.

[53] E. N. Dvorkin, K.-J. Bathe, A continuum mechanics based four-node shell element for general non-linear analysis, Engineering computations 1 (1) (1984) 77–88.